

Supplementary data

“Copolymer-co-morphology” Conception for Shape-Controlled Synthesis of Prussian Blue Analogues and as-Derived Spinel Oxides

Xuning Li,^{a,d} Lizhi Yuan,^{b,d} Junhu Wang,^{*,a} Luhua Jiang,^{*,b} Alexandre I. Rykov,^a Dénes L. Nagy,^e
Csilla Bogdán,^e Mamdouh A. Ahmed,^f Kaiyue Zhu,^{c,d} Gongquan Sun,^b and Weishen Yang^c

^a*Mössbauer Effect Data Center, Dalian Institute of Chemical Physics, Chinese Academy of Sciences, Dalian 116023, China*

^b*Dalian National Laboratory for Clean Energy, Dalian Institute of Chemical Physics, Chinese Academy of Sciences, Dalian 116023, China*

^c*State Key Laboratory of Catalysis, Dalian Institute of Chemical Physics, Chinese Academy of Sciences, Dalian 116023, China*

^d*University of Chinese Academy of Sciences, Beijing 100049, China*

^e*Institute for Particle and Nuclear Physics, Wigner Research Centre for Physics, Hungarian Academy of Sciences, H-1525 Budapest, P.O.B. 49, Hungary*

^f*Physics Department, Faculty of Science, Al Azhar University, Nasr City, Cairo, Egypt*

*Corresponding author. Tel: +86-411-84379159; Email: wangjh@dicp.ac.cn, sunshine@dicp.ac.cn.

Text S1. The detailed explanation of the binomial model for the 77 K ⁵⁷Fe Mössbauer spectra fitment.

The assumption is that the hyperfine magnetic field (H_{hf}) at octahedral-site (B-site) Fe nuclei is a function of the occupation of the six nearest tetrahedral-site (A-site) Fe^{III} and non-iron ions. Then the intensity ratio of the different B-site peaks can be calculated since it is proportional to the ratio of the probabilities of the different surroundings. So we have:

$$P(k) = \sum_{k=0}^6 \binom{6}{k} x^k (1-x)^{6-k} \quad (1)$$

Where $P(k)$ is the relative intensity of the B peak with k Fe^{III} ions in the nearest-neighbor A sites and x is the concentration of in Fe^{III} ions in A sites. The plots of binomial distribution for B-site Fe^{III} are shown in Figure S14. At the same time, the H_{hf} at A-site Fe nuclei is a function of the occupation of the nearest twelve B-site Fe^{III} and the other ions, so we have:

$$P(k) = \sum_{k=0}^{12} \binom{12}{k} x^k (1-x)^{12-k} \quad (2)$$

The plots of binomial distribution for A-site Fe^{III} are shown in Figure S15. The binomial distribution could well keep its shape when a fraction of ions is magnetic, and another fraction is not. In the present case, all ions are magnetic; although the Fe-Fe interactions are strongest, the weaker Fe-Co and Fe-Mn and the weakest Co-Mn interaction also play a role. These non-uniformity interactions may induce the deformation into the shape of $P(H_{hf})$ compared to the binomial distribution. However, for Mn_{0.3}Fe_{1.5}Co_{1.2}O₄ nano-dices, which contain a large percentage of Fe, the $P(H_{hf})$ is likely to be determined mainly by Fe-Fe interactions. Therefore, the fitted H_{hf} distribution of the A-site and B-site Fe in Mn_{0.3}Fe_{1.5}Co_{1.2}O₄ nano-dices follows the binomial distribution very well (Figure S16), indicating the approximate suitability of binomial model for analyzing the cation distribution in the samples.

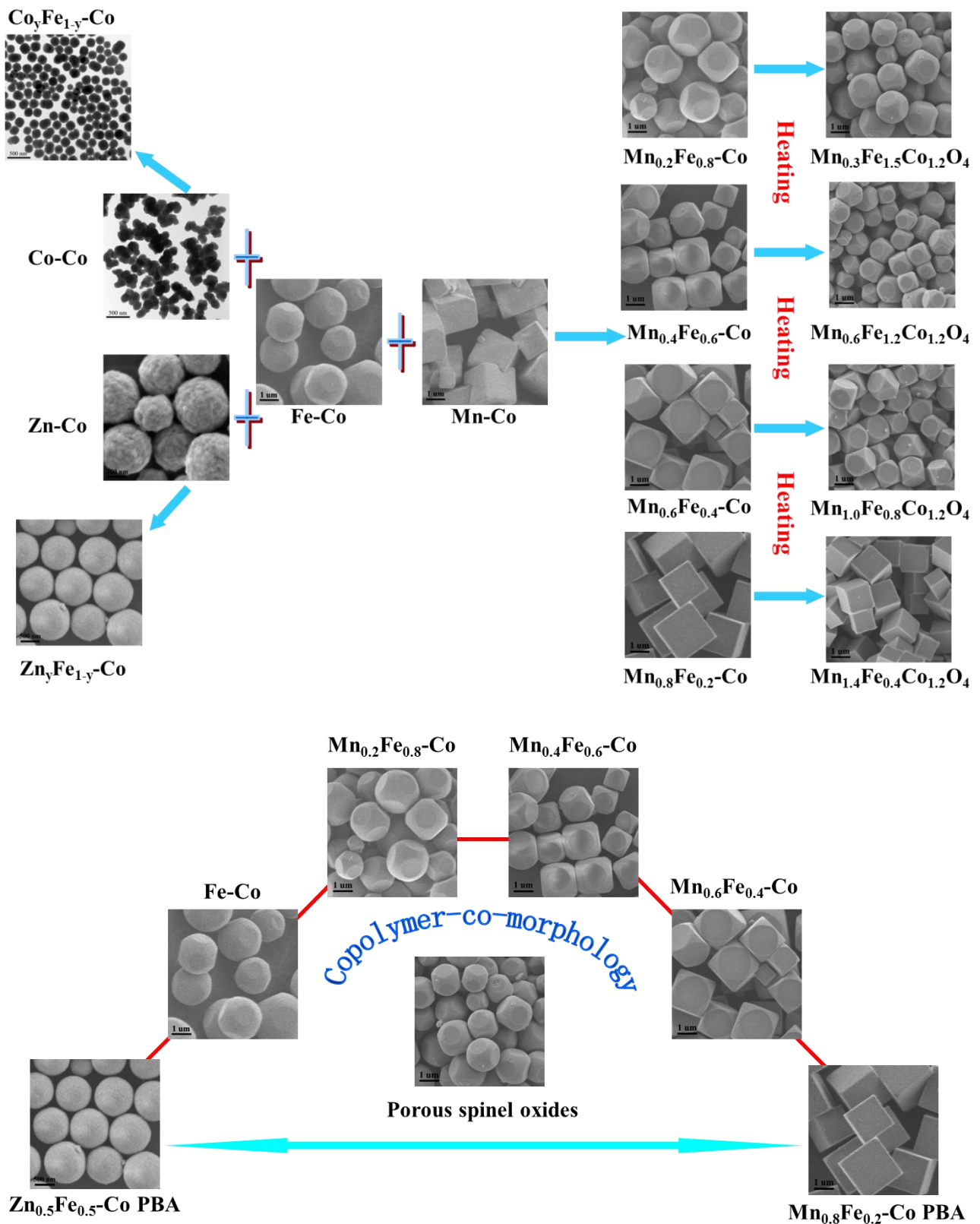


Figure S1. Schematic illustration of the “copolymer-co-morphology” conception for preparation of $\text{M}_y\text{Fe}_{1-y}\text{-Co}$ PBAs with controlled morphology.

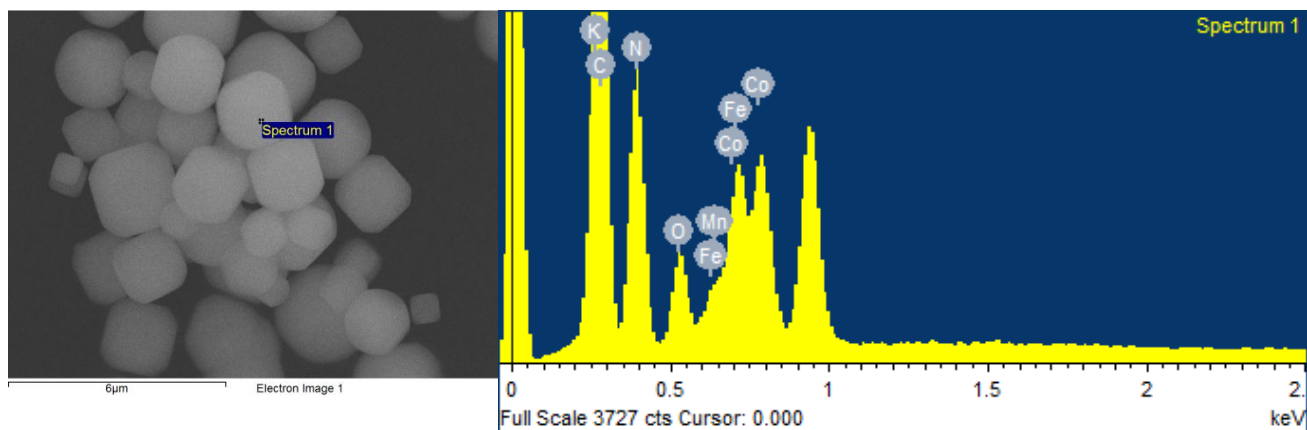


Figure S2. EDS element data of $\text{Mn}_{0.2}\text{Fe}_{0.8}\text{-Co PBA}$

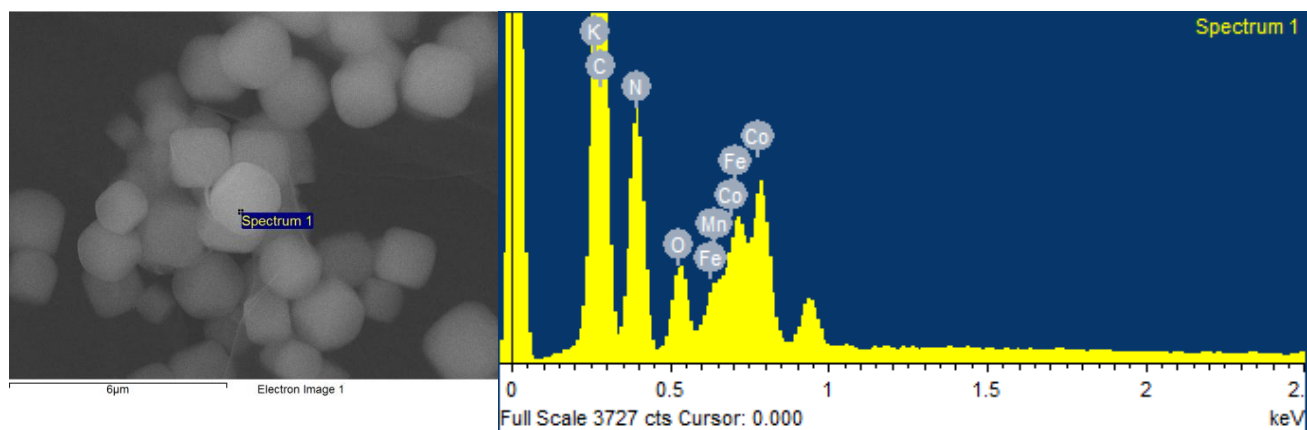


Figure S3. EDS element data of $\text{Mn}_{0.4}\text{Fe}_{0.6}\text{-Co PBA}$

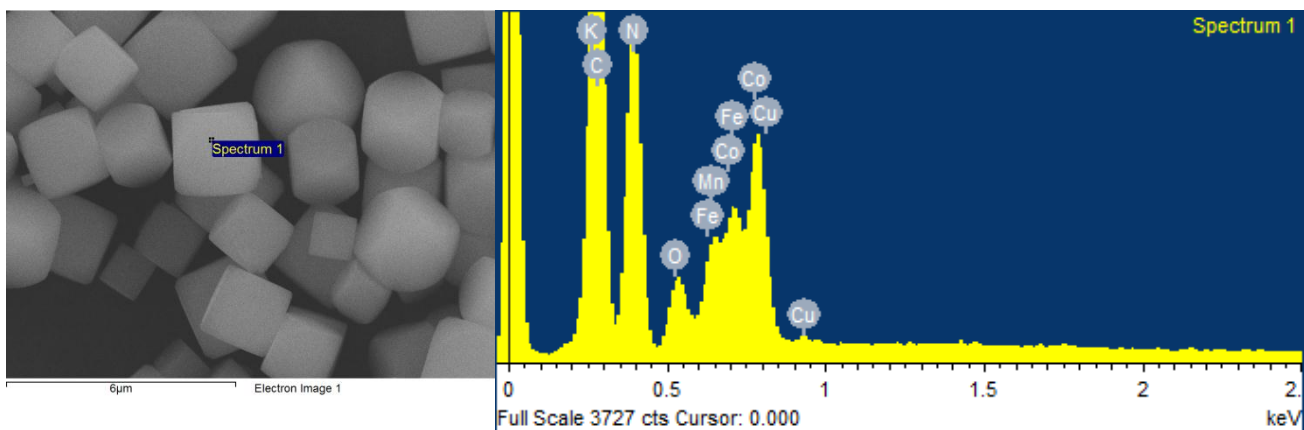


Figure S4. EDS element data of Mn_{0.6}Fe_{0.4}-Co PBA

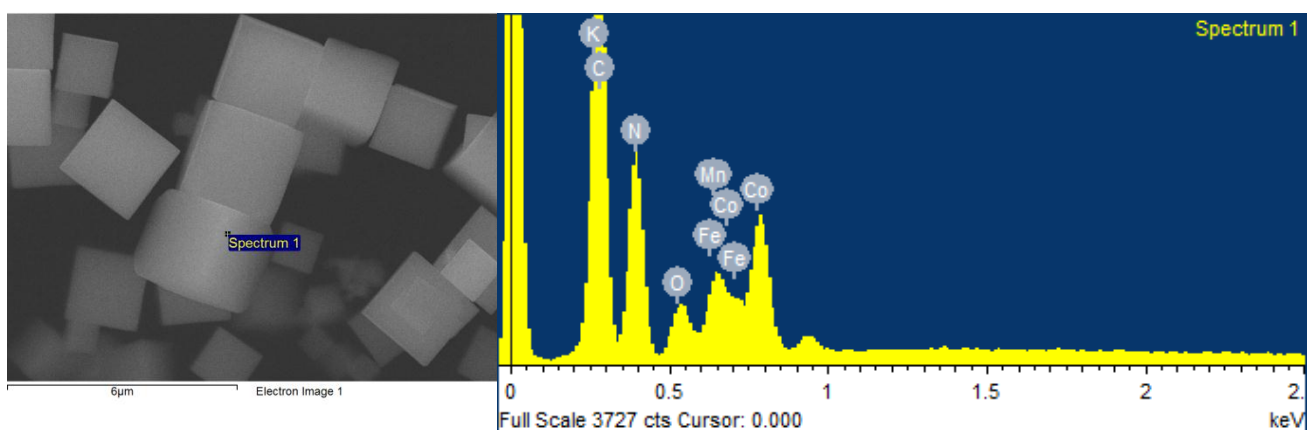


Figure S5. EDS element data of Mn_{0.8}Fe_{0.2}-Co PBA

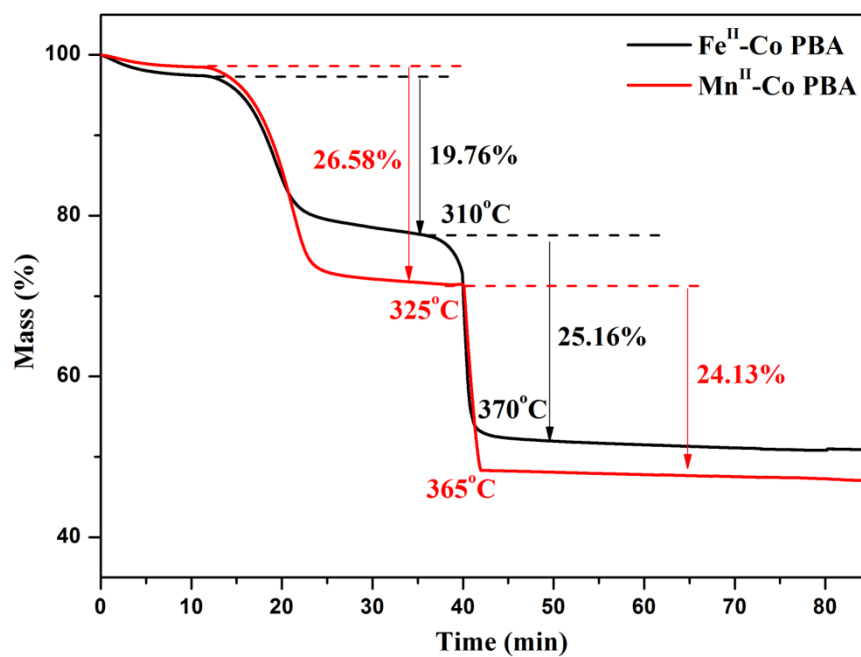


Figure S6. TG analysis of Fe-Co and Mn-Co PBAs.

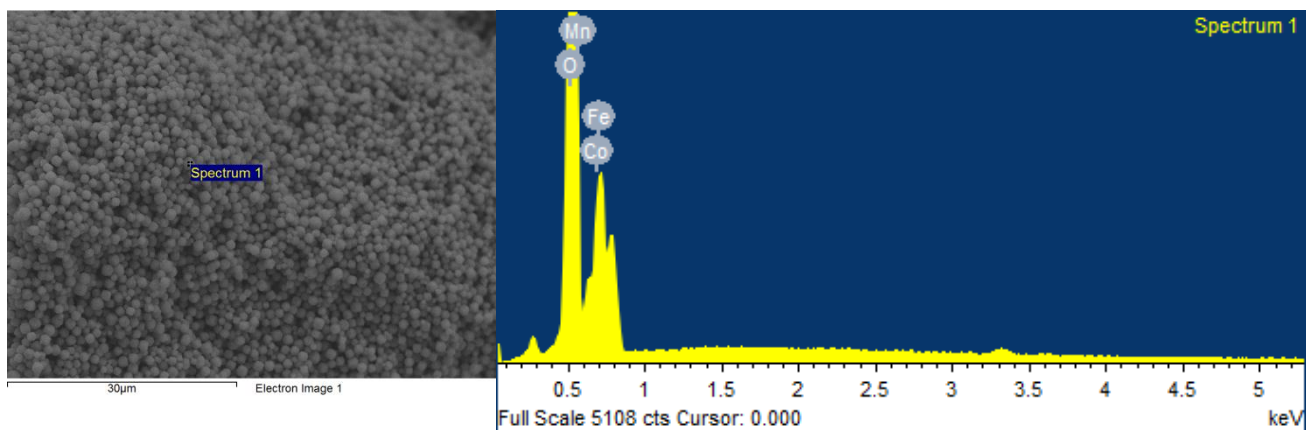


Figure S7. EDS element data of $\text{Mn}_{0.3}\text{Fe}_{1.5}\text{Co}_{1.2}\text{O}_4$.

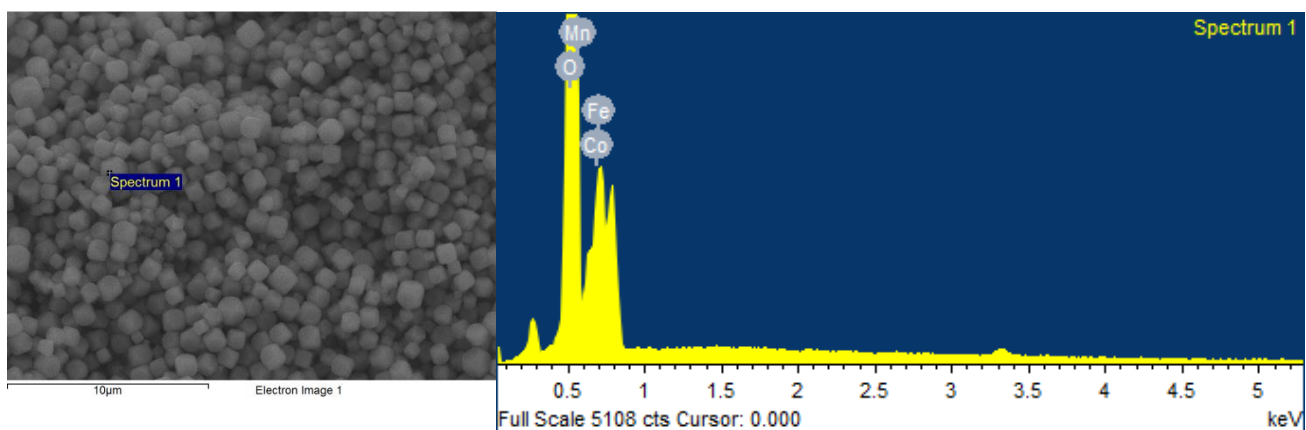


Figure S8. EDS element data of $\text{Mn}_{0.6}\text{Fe}_{1.2}\text{Co}_{1.2}\text{O}_4$.

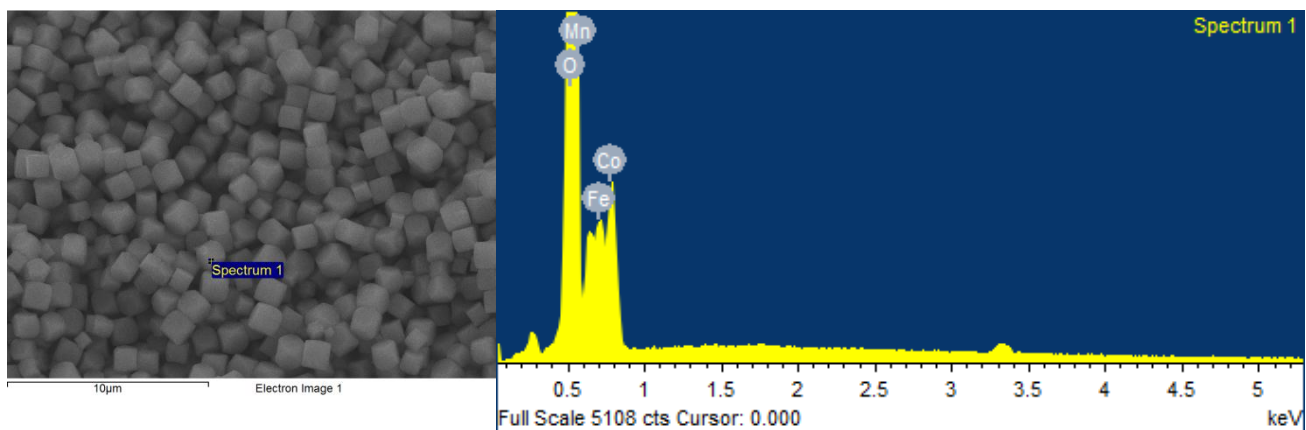


Figure S9. EDS element data of $\text{Mn}_{1.0}\text{Fe}_{0.8}\text{Co}_{1.2}\text{O}_4$.

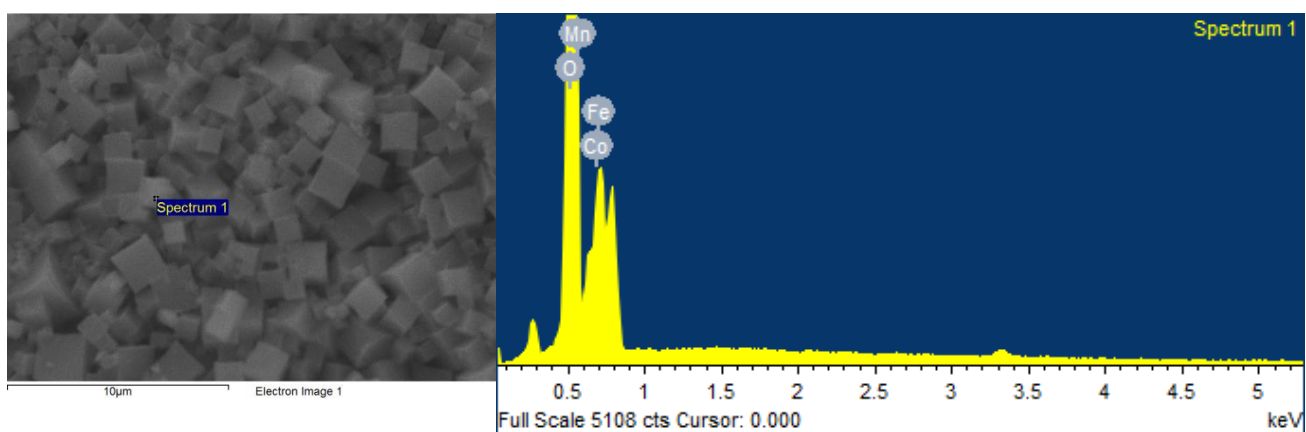


Figure S10. EDS element data of $\text{Mn}_{1.4}\text{Fe}_{0.4}\text{Co}_{1.2}\text{O}_4$.

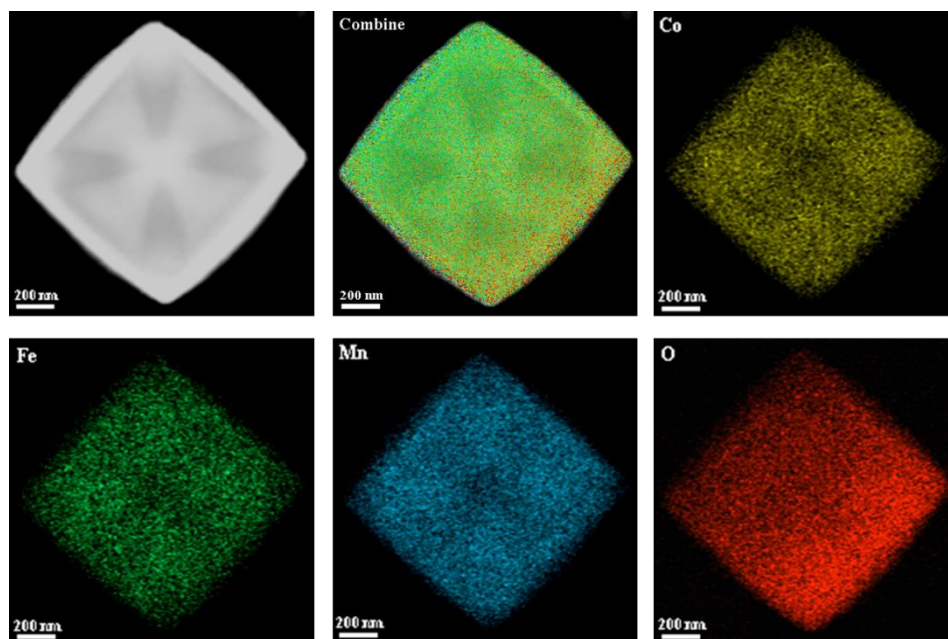


Figure S11. EDX mappings of porous $\text{Mn}_{1.4}\text{Fe}_{0.4}\text{Co}_{1.2}\text{O}_4$.

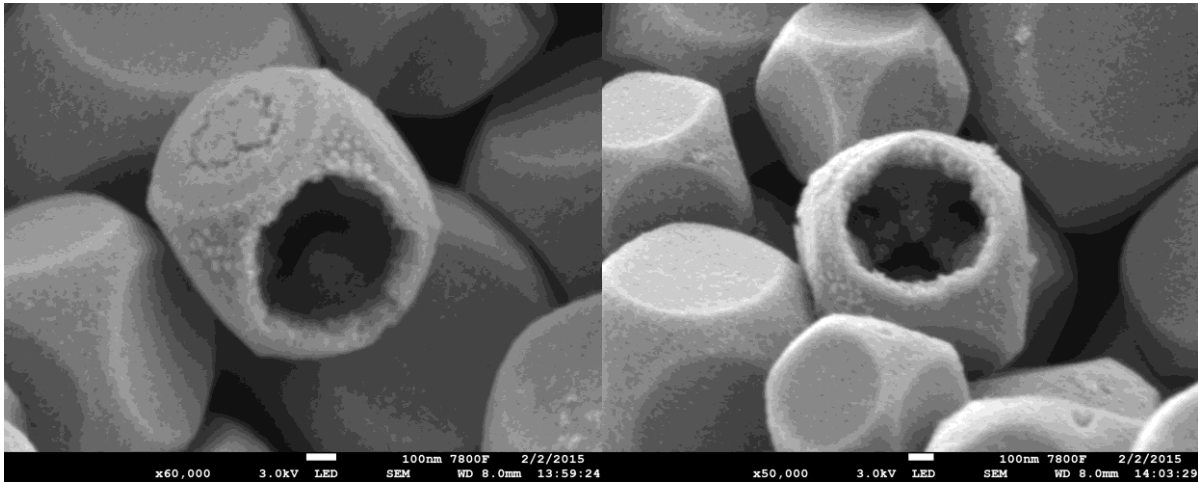


Figure S12. FESEM images of one broken particle of $\text{Mn}_{0.6}\text{Fe}_{1.2}\text{Co}_{1.2}\text{O}_4$ nano-dices.

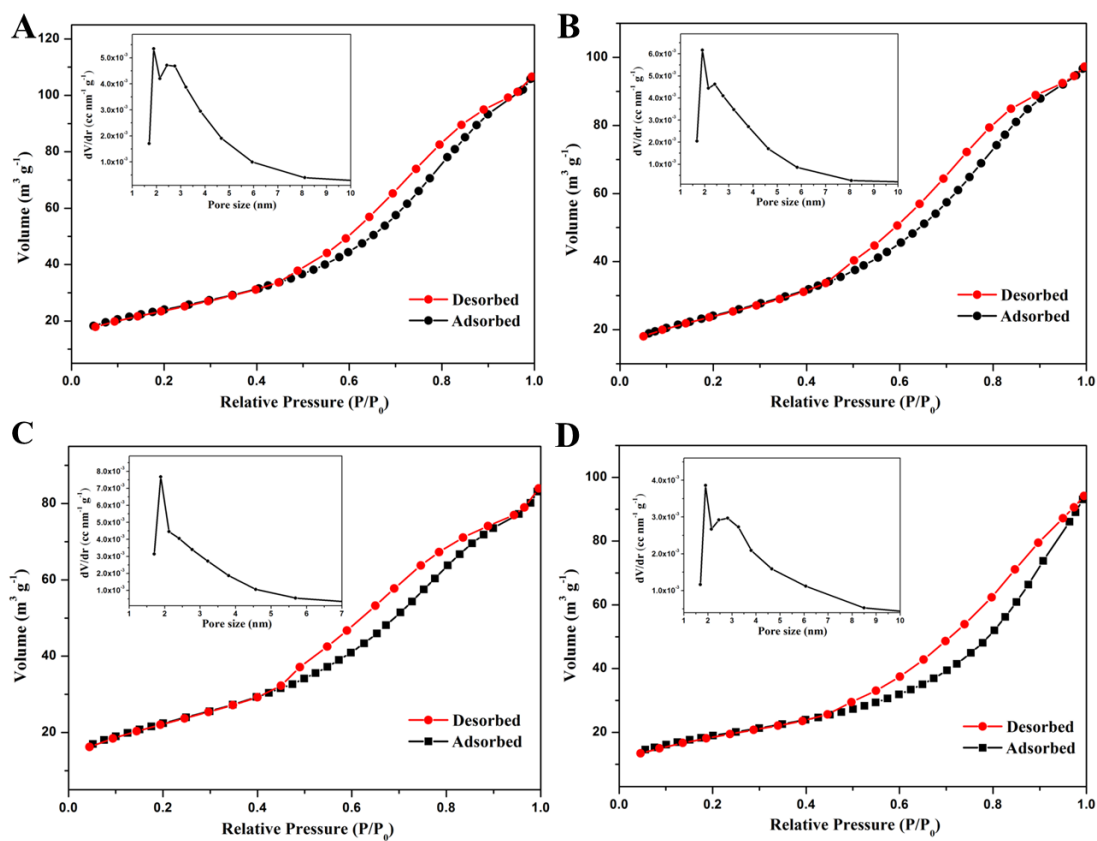


Figure S13. Nitrogen adsorption-desorption isotherms and pore size distribution (inset) of (A)

$\text{Mn}_{0.3}\text{Fe}_{1.5}\text{Co}_{1.2}\text{O}_4$; (B) $\text{Mn}_{0.6}\text{Fe}_{1.2}\text{Co}_{1.2}\text{O}_4$; (C) $\text{Mn}_{1.0}\text{Fe}_{0.8}\text{Co}_{1.2}\text{O}_4$; (D) $\text{Mn}_{1.4}\text{Fe}_{0.4}\text{Co}_{1.2}\text{O}_4$.

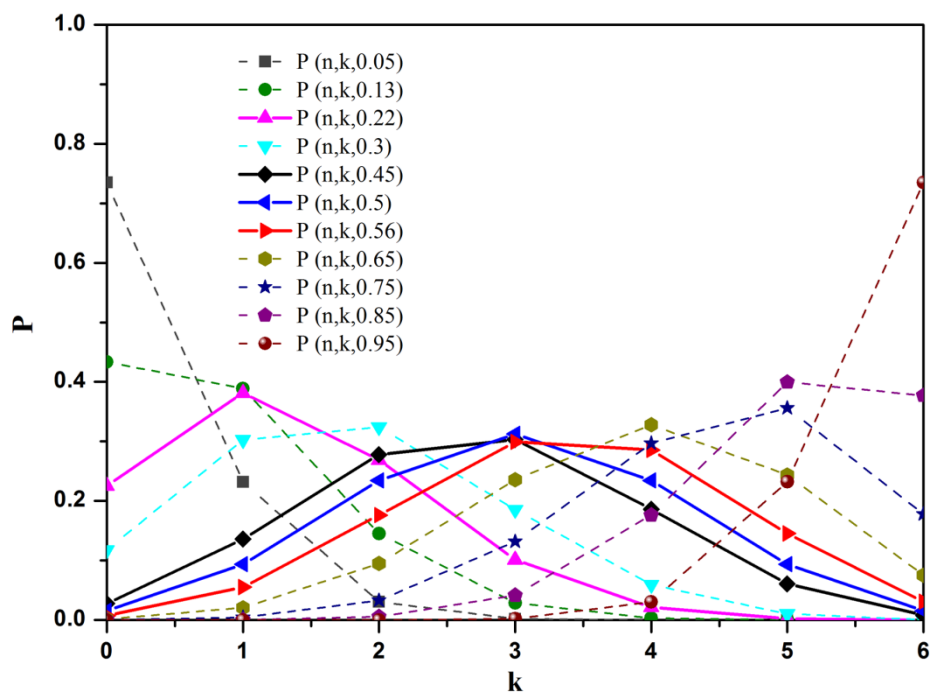


Figure S14. Plots of binomial distribution for B-site Fe^{III}. The black, red, blue, and magenta are the binomial distribution of the B-site Fe^{III} in Mn_{0.3}Fe_{1.5}Co_{1.2}O₄, Mn_{0.6}Fe_{1.2}Co_{1.2}O₄, Mn_{1.0}Fe_{0.8}Co_{1.2}O₄, and Mn_{1.4}Fe_{0.4}Co_{1.2}O₄, respectively.

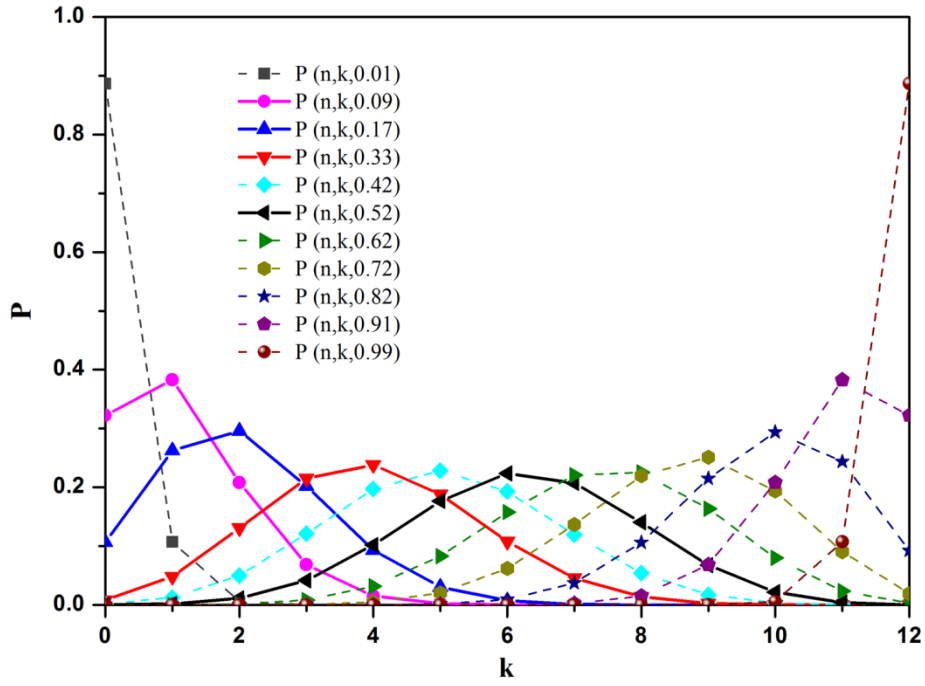


Figure S15. Plots of binomial distribution for A-site Fe^{III} . The black, red, blue, and magenta are the binomial distribution of the A-site Fe^{III} in $\text{Mn}_{0.3}\text{Fe}_{1.5}\text{Co}_{1.2}\text{O}_4$, $\text{Mn}_{0.6}\text{Fe}_{1.2}\text{Co}_{1.2}\text{O}_4$, $\text{Mn}_{1.0}\text{Fe}_{0.8}\text{Co}_{1.2}\text{O}_4$, and $\text{Mn}_{1.4}\text{Fe}_{0.4}\text{Co}_{1.2}\text{O}_4$, respectively.

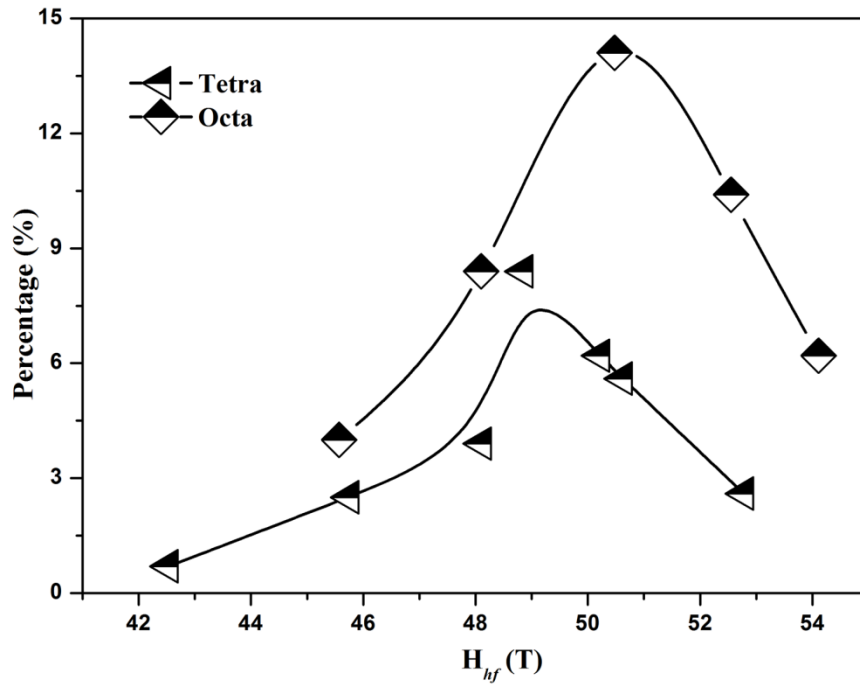


Figure S16. Magnetic field distribution of the fitted sub-spectra for Mn_{0.3}Fe_{1.5}Co_{1.2}O₄ nano-dices.

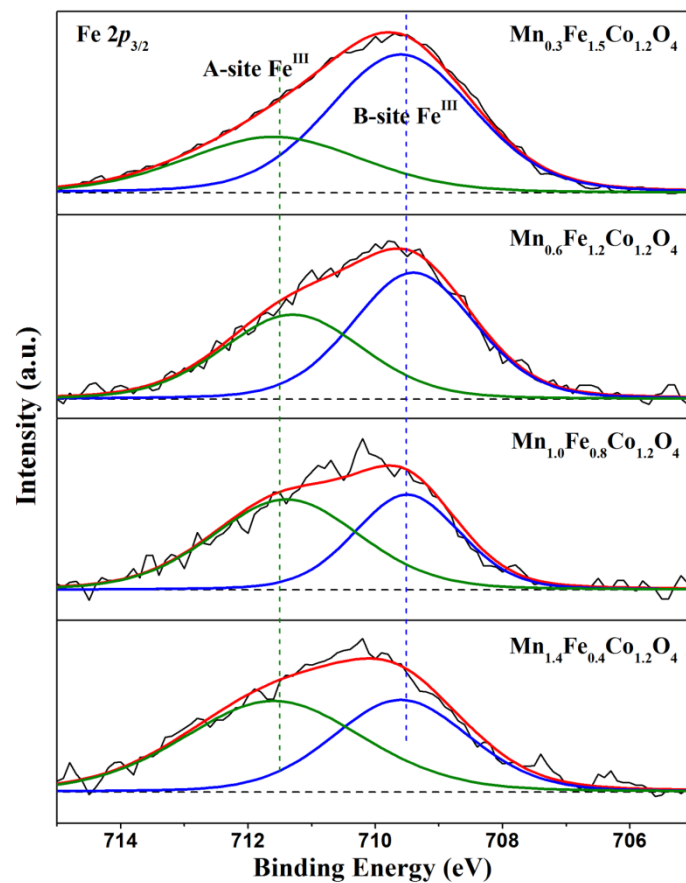


Figure S17. The high resolution XPS spectra of Fe $2p_{3/2}$ on $\text{Mn}_x\text{Fe}_{1.8-x}\text{Co}_{1.2}\text{O}_4$ surface.

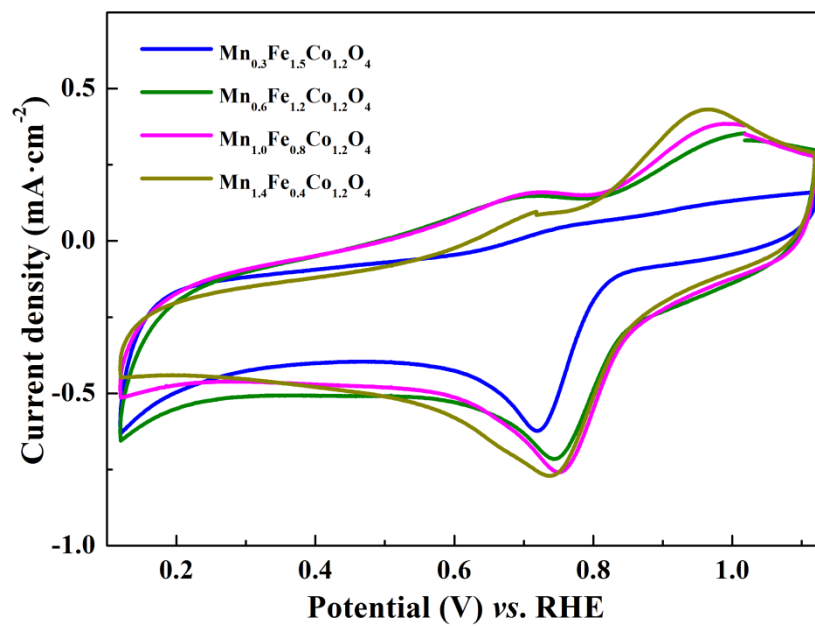


Figure S18. CV curves of Mn_xFe_{1.8-x}Co_{1.2}O₄ nano-dices. Electrolyte: O₂-saturated 0.1 M NaOH solution.

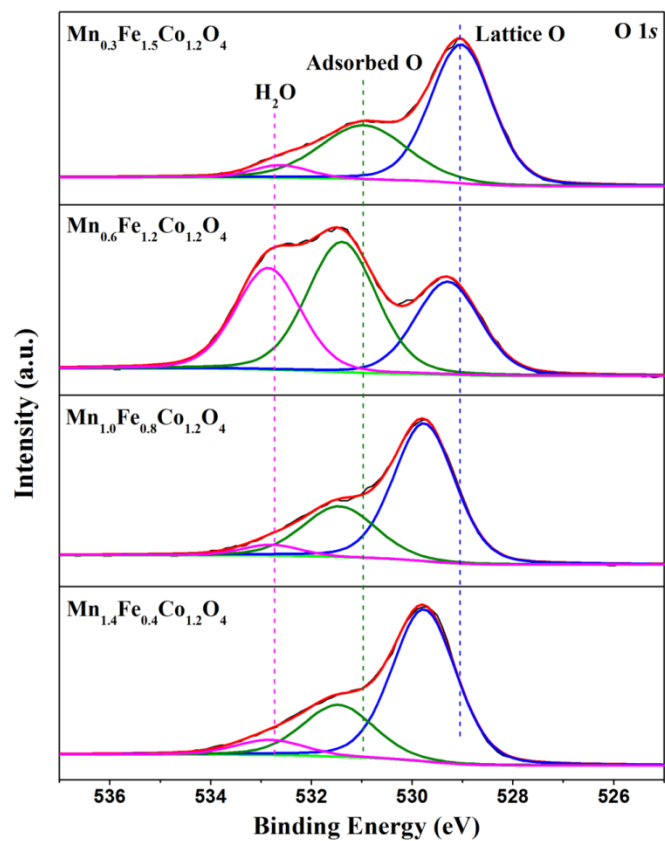


Figure S19. The high resolution XPS spectra of O 1s on Mn_xFe_{1.8-x}Co_{1.2}O₄ surface.

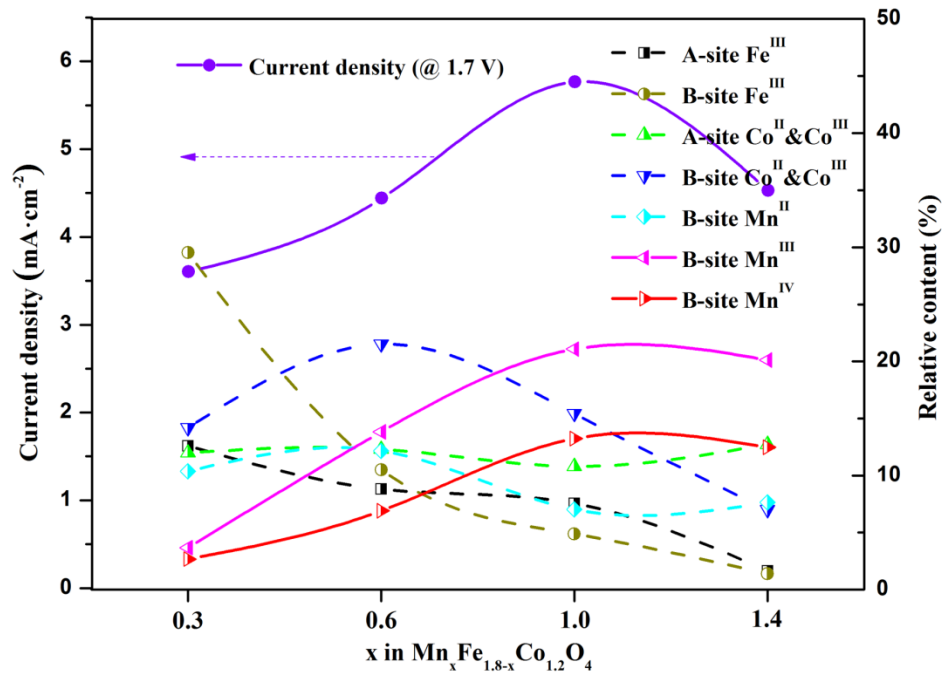


Fig. S20. Structure-function correlations between the OER activities and the relative contents of A-site or B-site M ions of $\text{Mn}_x\text{Fe}_{1.8-x}\text{Co}_{1.2}\text{O}_4$ nano-dices.

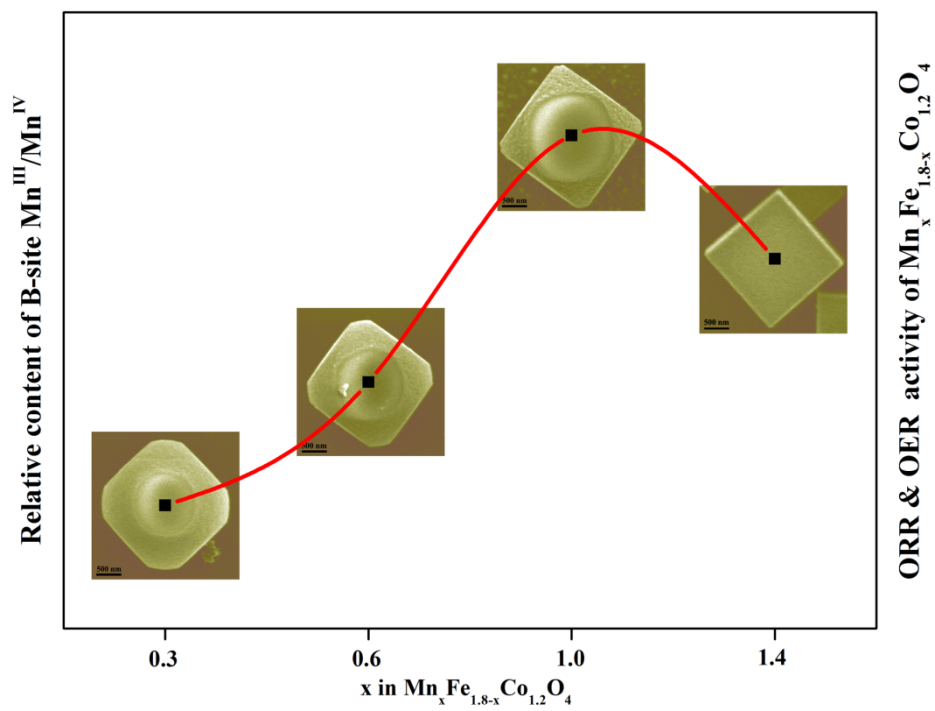


Fig. S21. The structure-function correlations between the ORR and OER activities and the relative content of B-site Mn^{III}/Mn^{IV} of Mn_xFe_{1.8-x}Co_{1.2}O₄ nano-dices.

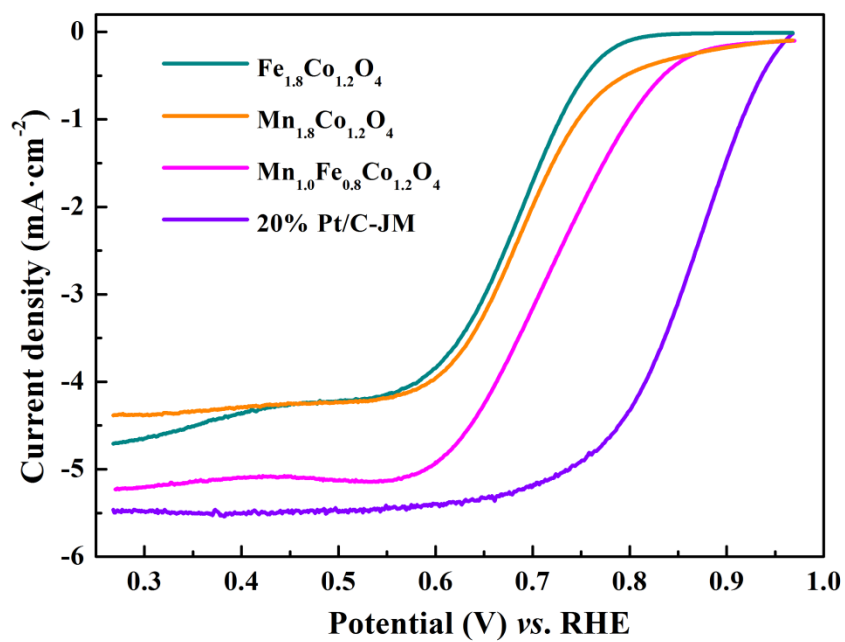


Fig. S22. ORR polarization curves of Mn_xFe_{1.8-x}Co_{1.2}O₄ nano-dices. The scan rate is 10 mV s⁻¹, and the rotation rate is 1600 rpm. Electrolyte: O₂-saturated 0.1 M NaOH solution.

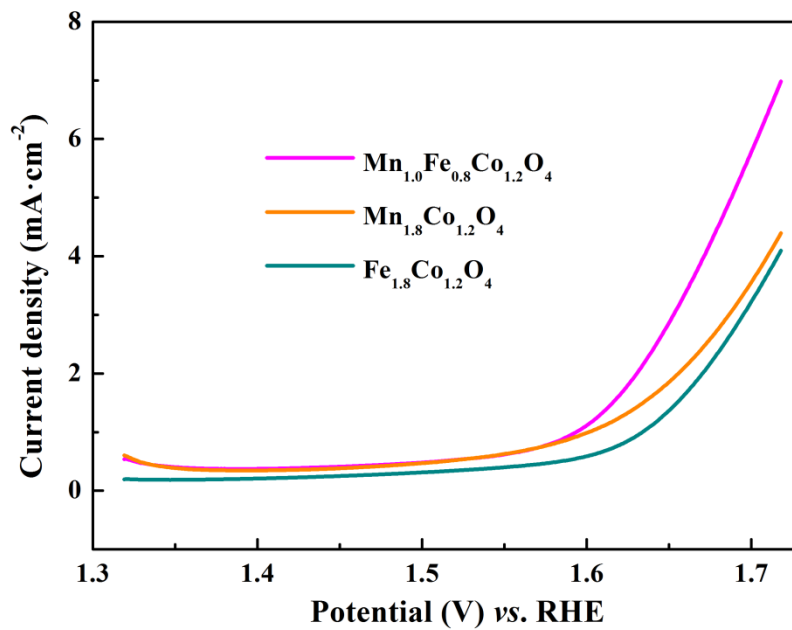


Fig. S23. OER polarization curves of $\text{Mn}_x\text{Fe}_{1.8-x}\text{Co}_{1.2}\text{O}_4$ nano-dices. The scan rate is 10 mV s^{-1} , and the rotation rate is 1600 rpm. Electrolyte: N_2 -saturated 0.1 M NaOH solution.

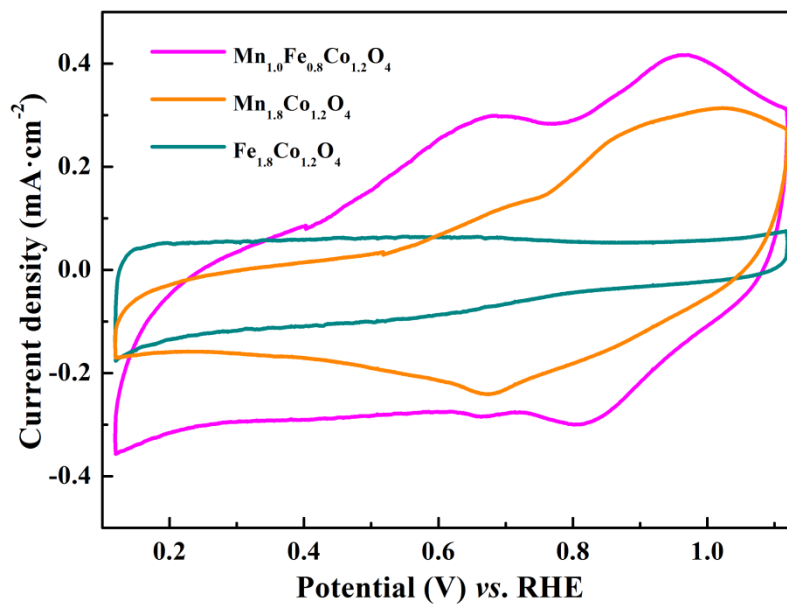


Figure S24. CV curves of $\text{Mn}_{1.0}\text{Fe}_{0.8}\text{Co}_{1.2}\text{O}_4$, $\text{Mn}_{1.8}\text{Co}_{1.2}\text{O}_4$ and $\text{Fe}_{1.8}\text{Co}_{1.2}\text{O}_4$. Electrolyte: N_2 -saturated 0.1 M NaOH solution.

Table S1. The chemical compositions of $\text{Mn}_y\text{Fe}_{1-y}\text{-Co}$ PBAs analyzed by EDS.

Element	$\text{Mn}_{0.3}\text{Fe}_{1.5}\text{Co}_{1.2}\text{O}_4$	$\text{Mn}_{0.6}\text{Fe}_{1.2}\text{Co}_{1.2}\text{O}_4$	$\text{Mn}_{1.0}\text{Fe}_{0.8}\text{Co}_{1.2}\text{O}_4$	$\text{Mn}_{1.4}\text{Fe}_{0.4}\text{Co}_{1.2}\text{O}_4$
C	44.54	44.24	40.84	43.68
N	41.99	41.94	47.57	43.57
O	8.24	8.65	6.32	5.60
Mn	0.42	0.87	1.49	3.08
Fe	2.63	2.09	1.52	1.04
Co	2.13	2.16	2.11	2.94

Table S2. The chemical compositions of $\text{Mn}_x\text{Fe}_{1.8-x}\text{Co}_{1.2}\text{O}_4$ nano-dices analyzed by EDS.

Element	$\text{Mn}_{0.2}\text{Fe}_{0.8}\text{-Co PBA}$	$\text{Mn}_{0.4}\text{Fe}_{0.6}\text{-Co PBA}$	$\text{Mn}_{0.6}\text{Fe}_{0.4}\text{-Co PBA}$	$\text{Mn}_{0.8}\text{Fe}_{0.2}\text{-Co PBA}$
O	69.20	72.48	70.63	72.83
Mn	3.23	5.18	9.56	12.57
Fe	15.29	11.23	8.09	3.63
Co	12.27	11.11	11.72	10.98

Table S3. The Mössbauer parameters obtained from 77 K Mössbauer measurements.

Sample	Site	IS (mm s ⁻¹)	H _{hf} (T)	%	Estimated Distribution
Mn _{0.3} Fe _{1.5} Co _{1.2} O ₄	A	0.32	42.5, 45.7, 48.1, 48.9, 50.2, 50.6, 52.8	29.9	(Fe _{0.45} Co _{0.55}) ^A
	B	0.49	43.6, 45.6, 48.1, 50.5, 52.5, 54.1	70.1	[Fe _{1.04} Mn _{0.31} Co _{0.65}] ^B
Mn _{0.6} Fe _{1.2} Co _{1.2} O ₄	A	0.36	39.8, 42.1, 44.4, 46.2, 48.0, 49.6, 51.3	45.6	(Fe _{0.56} Co _{0.44}) ^A
	B	0.51	39.9, 43.9, 46.6, 49.3, 51.6, 53.6	54.4	[Fe _{0.66} Mn _{0.56} Co _{0.77}] ^B
Mn _{1.0} Fe _{0.8} Co _{1.2} O ₄	A	0.42	37.4, 40.3, 43.2, 45.5, 47.4, 49.0, 50.5	60.8	(Fe _{0.50} Co _{0.50}) ^A
	B	0.53	30.3, 35.3, 38.9, 41.9, 45.4, 51.5	39.2	[Fe _{0.33} Mn _{0.98} Co _{0.70}] ^B
Mn _{1.4} Fe _{0.4} Co _{1.2} O ₄	A	0.40	29.0, 32.8, 36.1, 40.1, 42.6, 45.2, 47.6	53.9	(Fe _{0.22} Co _{0.78}) ^A
	B	0.52	18.8, 38.6, 41.6, 44.8, 47.2, 49.6	46.1	[Fe _{0.18} Mn _{1.39} Co _{0.43}] ^B

Experimental errors are ± 0.02 mm s⁻¹ for isomer shift (IS), ± 0.4 T for hyperfine field (H_{hf}) and 5% for relative area. IS is relative to α -Fe at room temperature.

Table S4. The Mössbauer parameters obtained from RT Mössbauer measurements.

Component	Site assignment	IS (mm s ⁻¹)	QS (mm s ⁻¹)	B_{hf} (T)	Γ (mm s ⁻¹)	Area (%)	
Mn _{0.3} Fe _{1.5} Co _{1.2} O ₄	A	Doublet (green)	0.36	0.62	-	0.68	11.3
		Sextets (cyan)	0.31	-0.03	45.	0.64/0.99/1.34	22.2
	B	Doublet (orange)	0.26	1.10	-	1.68	16.6
		Sextets (yellow)	0.29	-0.14	26.	0.85/3.27/5.70	49.8
Mn _{0.6} Fe _{1.2} Co _{1.2} O ₄	A	Doublet (green)	0.32	0.64	-	0.46	22.3
		Sextets (cyan)	0.30	-0.05	45.	0.54/1.04/1.55	22.4
	B	Doublet (orange)	0.30	0.94	-	1.35	29.7
		Sextets (yellow)	0.31	0.00	25.	0.53/2.35/4.17	25.6
Mn _{1.0} Fe _{0.8} Co _{1.2} O ₄	A	Doublet (green)	0.32	0.67	-	0.48	62.2
	B	Doublet (orange)	0.32	1.07	-	1.07	37.8
Mn _{1.4} Fe _{0.4} Co _{1.2} O ₄	A	Doublet (green)	0.31	0.53	-	0.40	50.0
	B	Doublet (orange)	0.33	0.88	-	0.49	50.0

Experimental errors are ± 0.02 mm s⁻¹ for isomer shift (IS), ± 0.03 mm s⁻¹ for quadrupole splitting (QS) and 3% for relative area. IS is relative to α -Fe at room temperature.

Table S5. The Half-wave potentials of the ORR curve, current densities @1.7V of the OER curve, and the relative contents of A-site or B-site M ions (Y %) of $Mn_xFe_{1.8-x}Co_{1.2}O_4$ nano-dices. Y % = Percentage of surface Y (obtained from XPS) * BET surface area * Percentage of site distribution (analyzed by Mössbauer spectra) * Percentage of different valance (analyzed by XPS).

	$Mn_{0.3}Fe_{1.5}Co_{1.2}O_4$	$Mn_{0.6}Fe_{1.2}Co_{1.2}O_4$	$Mn_{1.0}Fe_{0.8}Co_{1.2}O_4$	$Mn_{1.4}Fe_{0.4}Co_{1.2}O_4$
Half-wave potential (V)	0.68	0.70	0.73	0.71
Current density @1.7 V ($mA\ cm^{-2}$)	3.61	4.44	5.77	4.53
A-site Fe^{III} (%)	12.59	8.81	7.57	1.65
B-site Fe^{III} (%)	29.53	10.50	4.88	1.41
A-site Co (%)	11.99	12.31	10.80	12.73
B-site Co (%)	14.18	21.50	15.42	7.01
B-site Mn^{II} (%)	10.36	12.17	7.03	7.64
B-site Mn^{III} (%)	3.68	13.81	21.08	20.10
B-site Mn^{IV} (%)	2.67	6.90	13.23	12.46